ACS APPLIED MATERIALS & INTERFACES

Letter

www.acsami.org

Single-Crystalline ZnO Spherical Particles by Pulsed Laser Irradiation of Colloidal Nanoparticles for Ultraviolet Photodetection

H. Wang,*[,†] A. Pyatenko,[‡] N. Koshizaki,[‡] H. Moehwald,[†] and D. Shchukin[§]

[†]Max Planck Institute of Colloids and Interfaces, 14424 Potsdam, Germany

[‡]Nanosystem Research Institute (NRI), National Institute of Advanced Industrial Science and Technology (AIST), Central 5, 1-1-1 Higashi, Tsukuba, Ibaraki 305-8565, Japan

[§]Stephenson Institute for Renewable Energy, Department of Chemistry, University of Liverpool, Peach Street, Liverpool, L69 7ZF, United Kingdom

ABSTRACT: We report the formation and ultraviolet (UV) photodetection of single-crystalline spherical ZnO particles by pulsed laser irradiation of commercial ZnO nanoparticles in water. The phase and microstructure analysis before and after laser irradiation reveals a crystal size increase and shape transformation from irregular to spherical. Time-dependent laser irradiation confirmed that fusion is the reason for nanoparticle growth up to single-crystalline spherical particles. After rapid cooling, they maintain size and shape and possess unique optical and electrical properties. Because of the single-crystalline feature and smooth surfaces, high and selective sensing of ultraviolet light is observed.

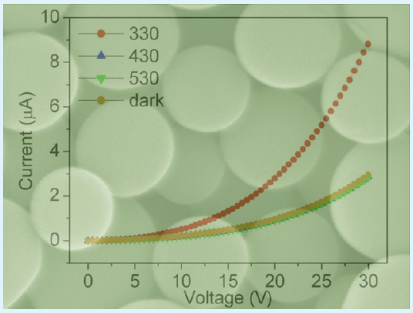

KEYWORDS: *ZnO, pulsed laser irradiation, photodetection, single crystalline, spherical particles*

INTRODUCTION

Semiconductor nanostructures, such as nanoparticles, nanowires, nanorods, and nanobelts, are attractive building blocks for a next generation of highly sensitive and selective sensors because of their high surface-to-volume ratios and diverse functions.[1−5] Because of the wide applications of photodetectors as binary switches in imaging techniques, light-wave communications, as well as in future memory storage and optoelectronic circuits, great efforts have been paid on development of photosensors, in which the function is based on the measurement of their optoelectronic response to incident irradiation.[6−8] A great number of one-dimensional nanostructures made by various material species such as NbO_2, CdS, ZnS has been explored.[6,9,10] Recently, one of the research interests has been focused on construction of photodetectors based on spherical particles, and preliminary encouraging results have been obtained for hollow ZnO and SnO_2 spheres.[11−13] However, the candidates of spherical particles used for photodetectors are always composed of secondary structures, e.g., nanoparticles, which inevitably create potential barriers for electron transfer in-between the subunits, thus deteriorating their optoelectronic performance. A possible solution could be increasing the crystallinity of spherical particles from polycrystalline to single-crystalline. However, creating single-crystalline spherical particles by using conventional heating is difficult when considering the crystalline nature of most semiconductors, which provides them anisotropic structures instead of spherical ones. Several unconventional approaches have been developed for crystalline spherical particles. For example, Xia et al. synthesized a range of low-melting-point metal spheres via quenching pre-melted spheres to retain their spherical morphology;[14,15] a well-controlled process of chemical etching towards preformed crystals to generate single-crystalline Au and Ag spheres.[16,17] However, these methods for creating single-crystalline spherical particles are only suitable for a narrow range of materials species.

Recently, we have developed a general synthetic approach to fabricate crystalline spherical particles with smooth surfaces by nanosecond pulsed laser irradiation of colloidal nanoparticles.[18] The unique temporally and spatially discontinuous heating mode involved in the laser irradiation process allows for preservation of the spherical shape of fully-melted particles upon sufficient laser energy absorption. Even more encouraging, single-crystalline spherical particles (such as TiO_2, Ag, silicon) can be accessed through continuous heating and solidification.[19−21] This inspires us to explore their photodetection characteristics. Zinc oxide, with band gap of 3.37 eV and a high exciton binding energy of 60 meV at room temperature, is an ideal candidate for visible-blind UV-light sensors and optoelectronic circuits.[22−24] Nevertheless, there have been no studies related to UV-detection by single-crystalline spherical ZnO particles. In this paper, we demonstrate the synthesis, characterization, and growth of ZnO crystalline spherical particles and our first attempt of using them as photodetectors with selective UV detection but blindness towards visible radiation.

Received: January 21, 2014
Accepted: February 14, 2014
Published: February 14, 2014

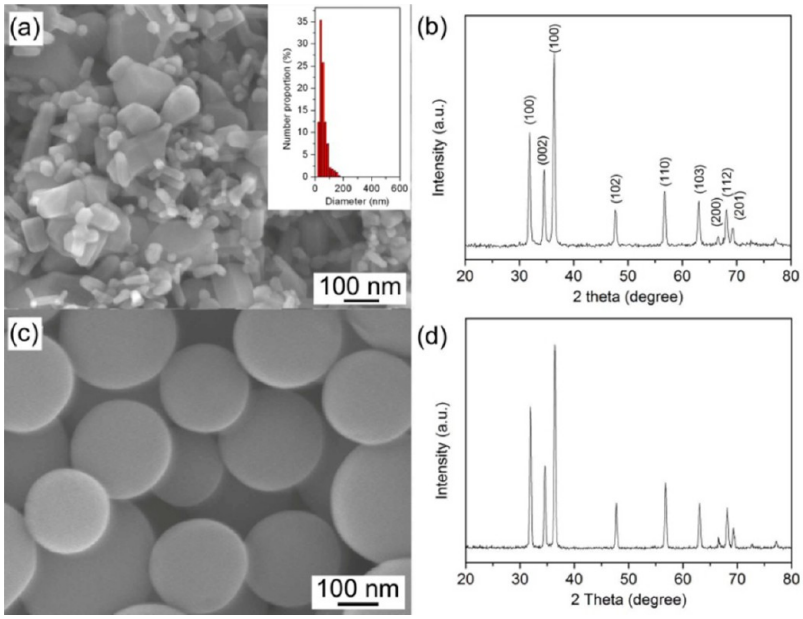

Figure 1. (a) FESEM image (inset: particle size distribution histogram) and (b) XRD pattern of ZnO raw nanoparticles. (c) FESEM image and (d) XRD pattern of spherical ZnO silver particles obtained by pulsed laser irradiation of ZnO nanoparticles in water (355 nm, 133 mJ/(pulse cm^2), 10 min, 0.8 mg/mL).

EXPERIMENTAL SECTION

Materials Synthesis. A Nd:YAG laser (Quanta Ray from Spectra-Physics; pulse width 10 ns, repetition rate 30 Hz) was used as the light source for pulsed laser irradiation. Typically, 0.8 mg of commercial ZnO nanoparticles (Aldrich, <100 nm, powder form) were first well-dispersed in 4 mL of water by ultrasonication. The mixture was then transferred to a sealed reaction cell and irradiated by an unfocused laser beam (133 mJ/(pulse cm^2)) for 10 min.

Characterization. The phase, morphology, and microstructure of the collected particles were measured using a powder diffractometer (Rigaku; Ultima IV/PSK), a field-emission scanning electron microscope (FESEM; Hitachi S4800), and a transmission electron microscope (TEM; JEOL 2010). X-ray photoelectron spectroscopic analysis (XPS; Perkin-Elmer PHI-5600ci) was performed for precipitates dried on Si substrates. An XPS depth profile analysis was used to investigate the composition distribution of ZnO spherical particles in radial direction. An ion gun was used to etch the material for a period of time. Each ion gun etch cycle exposes a new surface, and the XPS spectra recorded the compositions of these surfaces. The optical properties of suspensions with dispersed ZnO spherical particles were evaluated by UV−vis spectroscopy (Shimadzu UV-2100PC).

Photodetection Measurement. ZnO-spherical-particle photodetectors were assembled using Au microwires as masks and quartz as a substrate. An Au microwire (30 μm in diameter) was used as a mask to shadow some parts of a film of ZnO submicrometer spheres. A Ti/Au (20 nm/200 nm) film was deposited to cover the whole substrate by an electron-beam deposition process. After metal deposition the Au microwire was removed from the surface of the substrate. The current−voltage (I−V) characteristics of the ZnO-spherical-particle photodetectors was measured under illumination with light of different wavelengths or under dark conditions in ambient air at room temperature using an Advantest Picoammeter R8340A and a direct current (DC) voltage source R6144. The spectral response for different wavelengths was recorded using a xenon lamp (500 W). The time-dependent photocurrent response under 330 nm light illumination for the light-on and light-off states was recorded at an applied voltage of 30.0 V.

RESULTS AND DISCUSSION

Figure 1 presents the morphological and phase comparison of raw material and the product after pulsed laser irradiation of colloidal ZnO nanoparticles in water. Before laser irradiation, one observes that most of the ZnO nanoparticles are smaller than 100 nm (Figure 1a). The corresponding X-ray diffraction pattern (Figure 1b) indicates a hexagonal phase of the nanoparticles (JCPDS card No. 1-1167). Irradiating towards the raw nanoparticles dispersed in water for 10 min using a 355 nm laser (133 mJ/(pulse cm^2)) transformed the irregular ZnO nanoparticle into spherical ones (Figure 1c). The resultant spherical particles still have a hexagonal phase (JCPDS card No. 1-1167), indicating that there is no phase change after laser irradiation (Figure 1d). Careful examination reveals a slightly decreased diffraction peak width (Figure 1d) compared to that of raw material (Figure 1b). Crystal sizes were calculated from the FWHM (full width at half maximum) of the strongest diffraction peak (101) on the basis of the Debye Scherrer equation, indicating a crystal size increase (from 20.2 to 107 nm) by laser irradiation, which is in agreement with the FESEM observation presented in images a and c in Figure 1.

The low-magnification TEM image of the spherical particle in Figure 2a reveals its spherical shape and smooth surface. The selected area electron diffraction shown in the inset of Figure 2a indicates the single crystallinity of the ZnO spherical particles, which explains the decrease of the XRD peak width shown in Figure 1d. The UV−vis spectra of the ZnO nanoparticles in Figure 2b before and after laser irradiation show the different optical extinction of the two structures, in which each extinction spectrum is normalized to the maximum extinction value in the visible light range. The tails of the extinction curve for the resultant spherical ZnO particles in the long wavelength

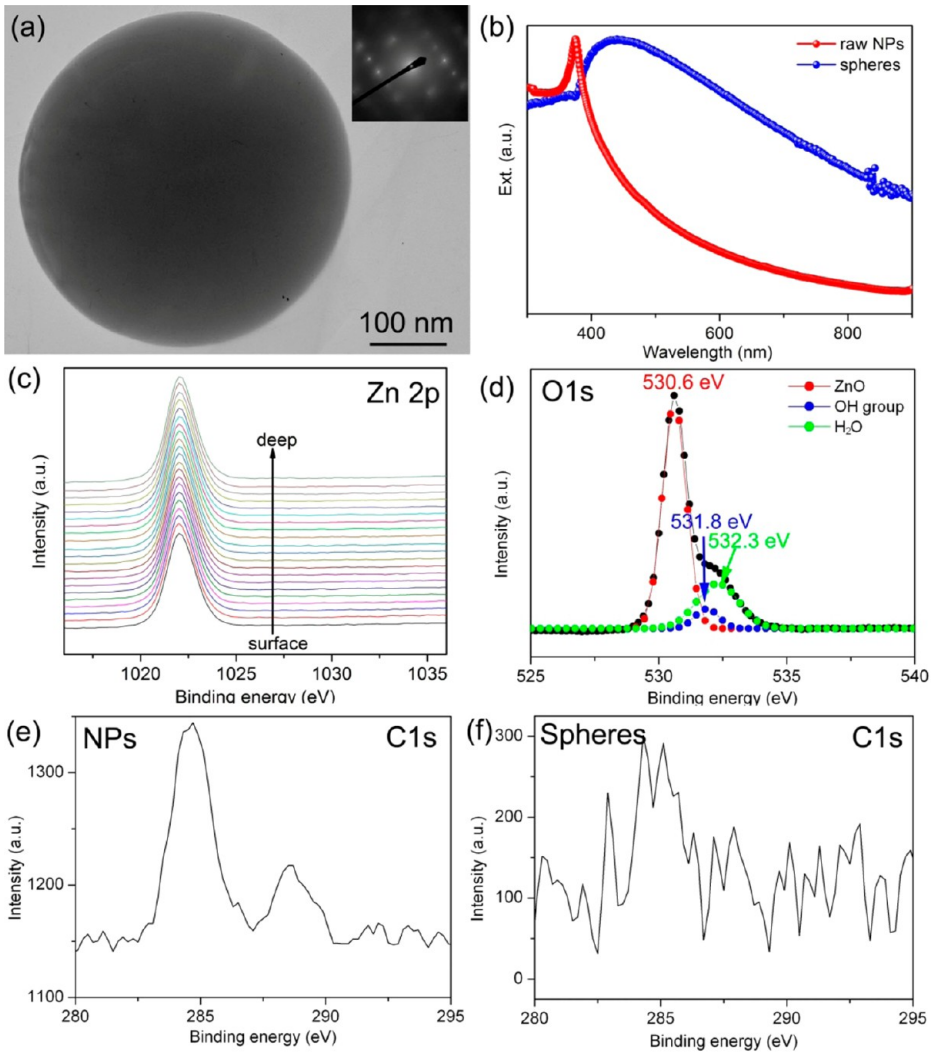

Figure 2. (a) TEM image and corresponding SAED pattern (inset) of ZnO spherical particles; (b) UV−vis extinction spectra ZnO nanoparticles and spherical particles; (c) XPS depth profile analysis of the Zn2p spectrum from the surface (bottom) to the bulk (top) of ZnO spherical particles; (d) XPS profile of O1s for ZnO spherical particles; XPS profiles of C1s for (e) ZnO raw nanoparticles and (f) spherical particles.

range are not hyperbolic (typical for Rayleigh scattering). This is understood if one considers that the size of the particles is comparable with the visible light wavelength, resulting in an obvious Mie scattering.[25]

XPS was used to characterize the surface states of the resultant ZnO spheres. All peak positions were corrected by the C 1s peak at 284.6 eV. Figure 2c depicts the XPS depth profiles of the ZnO spheres (Zn 2p), where the sputtering conditions for the first ten were 0.5 min at 1 kV and 1 min at 2 kV for the rest. It can be seen from Figure 2c that the binding energy of Zn 2p is constant from surface to bulk (around 130 nm depth), indicating the absence of other valence states of Zn. The XPS spectra of the O1s level with peak deconvolution analysis is shown in Figure 2d, which reveals the coexistence of three different states of oxygen. The peak at 530.6 eV is attributed to the Zn−O bond, while that at 531.8 eV is attributed to the OH group. The peak at 532.3 eV is ascribed to water adsorbed on the surface of spherical particles. Comparison with XPS analysis of the raw ZnO nanoparticles (not shown here) demonstrates no apparent change of the Zn 2p and O 1s states before and after laser irradiation. The notable difference before and after irradiation is due to the surface states of carbon. As demonstrated in Figure 2e, the surface carbon of ZnO nanoparticles before laser irradiation has two states. The one located at 284.6 eV is ascribed to physically absorbed carbon, the other one located at 288 eV is surface capping agent used for ZnO nanoparticle preparation. After laser irradiation, as shown in Figure 2f, the surface carbon was removed. This indicates, on the one hand, that the surface carbon was ablated because of the high temperature generated at the ZnO spheres melted upon laser absorption and, on the other hand, the ZnO spheres possess low physical absorption of carbon because of their smooth surfaces.

To figure out how ZnO spherical particles grow from raw nanoparticles, time-dependent laser irradiation was performed in water. As seen in Figure 3a, pulsed laser irradiation of ZnO nanoparticles for 30 s results in a small number of spherical particles with diameters below 100 nm, but the product is dominated by raw nanoparticles. If the laser irradiation time is increased to 60 s, the number of raw nanoparticles is significantly decreased (Figure 3b). Careful examination of the surfaces of the formed spherical particles at this stage reveals that the spherical particles are combined from several particles with irregular shape, which can be evidenced by the

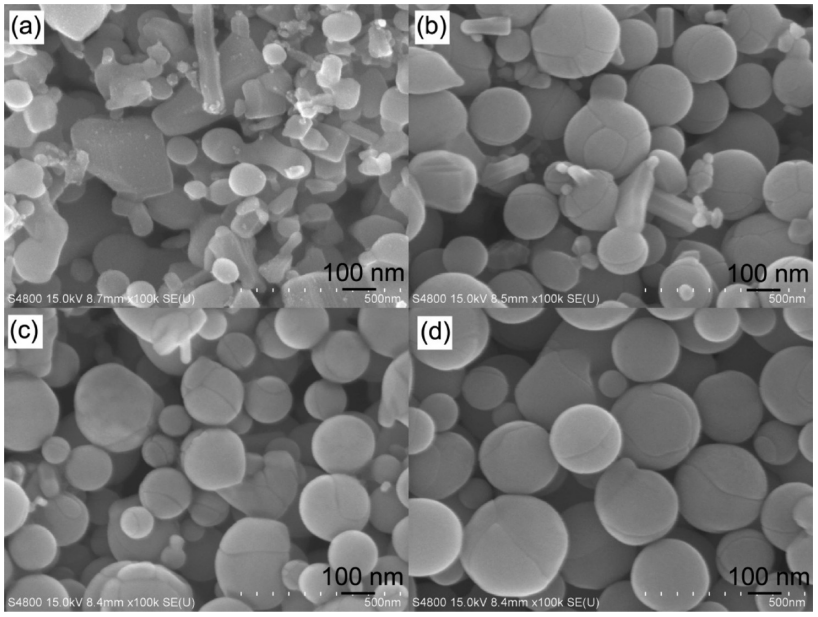

Figure 3. FESEM images of ZnO obtained by laser irradiation of commercial ZnO nanoparticles with different laser irradiation time (third harmonic, in water, 133 mJ/(pulse cm^2)): (a) 30 s, (b) 60 s, (c) 120 s, (d) 5 min.

apparent crystal boundaries on the surfaces. When further prolonging the irradiation time to 120 s, the product is dominated by solidified spherical particles (Figure 3c). After laser irradiation for 5 min, the product exhibits more homogeneous size distribution (Figure 3d), whereas crystal boundaries are still visible. Finally, after laser irradiation for 10 min, single crystalline spherical particles with smooth surfaces are seen (Figure 1c), indicating that single-crystal submicrometer spheres are formed by numerous heating, fusion, and solidification cycles caused by pulsed laser irradiation.

Spherical particles of ZnO are always formed when the input pulsed laser fluence is tuned from 67 to 133 mJ/(pulse cm^2), and the average sizes of resultant spherical particles increase accordingly.[26−28] However, there is a size limit for the resultant spherical particles at fixed laser fluence, indicating that they cannot grow by fusion endlessly, as the input laser energy directly determines the size of fully-melted particles. In pulsed laser irradiation of colloidal nanoparticles, the particle heating-melting-evaporation mechanism can be applicable for the nanosecond laser-colloidal nanoparticle interaction process.[29,30] The laser energy absorbed by the ZnO nanoparticle is assumed to heat the nanoparticles to start melting, full melting, start evaporation, or full evaporation of the nanoparticles,[29,30] as described in eq 1

$$Q_{abs} = J\sigma_{abs}^{\lambda} = m_p \int_{T_0}^{T_m} c_p^s(T)dT + m_p\Delta H_m + m_p \int_{T_m}^{T_b} c_p^l(T)dT + m_p\Delta H_{ev} \quad (1)$$

where $J = E_0/S_0$ is the fluence of a laser beam with pulse energy $E_0$and cross-section S_0, σ_{abs}^{λ} is the particle absorption cross-section, c_p^s and c_p^l are the particle heat capacities in the solid and liquid states, $m_p = \rho_p\pi d_p^3/6$ is the particle mass, T_0 is the particle initial temperature, T_m is the melting temperature, T_b is the boiling temperature, ΔH_m is the heat of melting, and ΔH_{ev} is the heat of evaporation. Depending on how much laser energy is absorbed (Q_{abs}), a pulsed laser will heat a particle from T_0 to the melting point T_m, to full melting, to the boiling point T_b, or to full evaporation, where full melting of nanoparticles corresponds to the formation of spherical particles with smooth surfaces.[31] The physical and thermodynamic constants used in eq 1 were adopted from literature.[32]

For the calculation we assume that during the pulse time there is no heat flux into the liquid environment. Figure 4

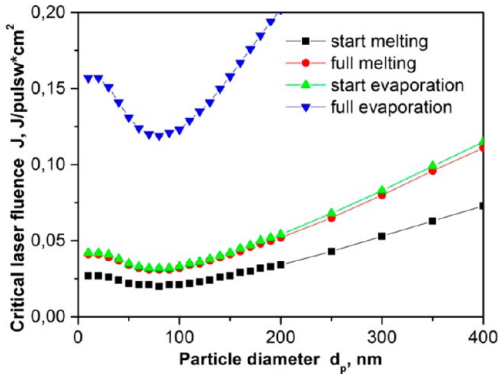

Figure 4. Required laser fluence J of a single pulse for ZnO vs. particle size to heat an individual spherical particle to start melting, full melting, start evaporation and full evaporation, using the pulsed laser (355 nm).

depicts our result (355 nm), in which both larger and smaller particles need high energy to fully melt, similar to the case of the CuO system.[33] For particles with size larger than 100 nm, it can be observed that higher laser fluence will result in full melting of much larger particles; that is, the size of a spherical droplet increases at higher laser fluence, and this could explain why experimentally increasing the laser fluence leads to the increase in the sizes of resultant spherical particles.

Liquid medium is an important parameter for accessing ZnO spherical particles. It was found that when we increased the laser fluence above 100 mJ/(pulse cm^2) in organic solvents,

such as acetone, the product was dominated by nanoparticles with an average size below 10 nm (Figure 5a). This is a typical

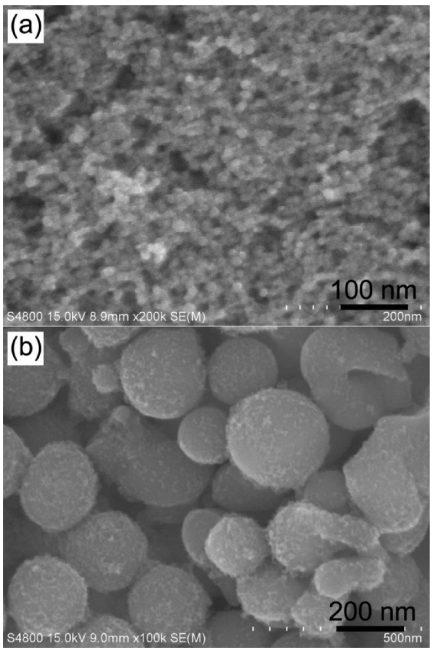

Figure 5. FESEM image of the product of ZnO nanoparticles in acetone after irradiation at 355 nm for 10 min: (a) 100 mJ/(pulse cm^2); (b) 50 mJ/(pulse cm^2).

size-reduction process in pulsed laser irradiation, where the production of much smaller nanoparticles is due to the evaporation of raw nanoparticles upon sufficient laser absorption.[34] At much lower laser fluence, e.g., 50 mJ/(pulse cm^2), nanoparticles with the size smaller than that of raw materials are produced together with the spherical particles, as seen in Figure 5b. This could be explained by the nearly overlapping of the two calculated curves of full-melting (red curve) and start of evaporation (green curve). On the other hand, the high temperature generated at the melted particle surface could lead to the decomposition of the surrounding acetone into reductive gases, e.g., C_2H_2,[35] which can reduce ZnO to Zn. As Zn has much lower melting and boiling points than ZnO, the laser energy that melts ZnO could lead to the evaporation of Zn, which produces much smaller nanoparticles.

It should be noted that pulsed laser heating is different from conventional heating, which is usually based on black-body radiation. When a pulsed laser is applied to the ZnO colloidal solution, it directly and intensively heats the nanoparticles and not the solvent, as thermal conduction into the sovent is rather slow, thus easily achieving the full melting of nanoparticles even at room temperature and in normal liquids.[18] When the laser beam heats the nanoparticles with pulse width of 10 ns and repetition rate of 10 Hz, instantaneous heating can be completed within 10 ns, followed by subsequent quenching that usually takes 1×10^{-6} to 1×10^{-4} s.[31] Therefore, pulsed laser heating is unique as it permits the full melting of raw nanoparticles to spherical particles that subsequently retain their spherical shape due to fast cooling, which can effectively inhibit the anisotropic crystal growth of ZnO.

The resulting ZnO spherical particles possess high crystallinity and smooth surfaces, where abundant dangling bonds should be produced on the curved surfaces, thus providing a richness of surface trap states that could efficiently prolong the photocarrier lifetime.[36] In this regard, we analyzed the photodetection behaviour of the crystalline ZnO spherical particles. Figure 6a presents a schematic diagram of the device configuration for measuring the photocurrent of ZnO submicrometer spheres, by monochromatic vertical illumination on the spherical particles, and the corresponding $I-V$ output is recorded by using a two-probe method. The SEM image of the device made up of ZnO spherical particles is

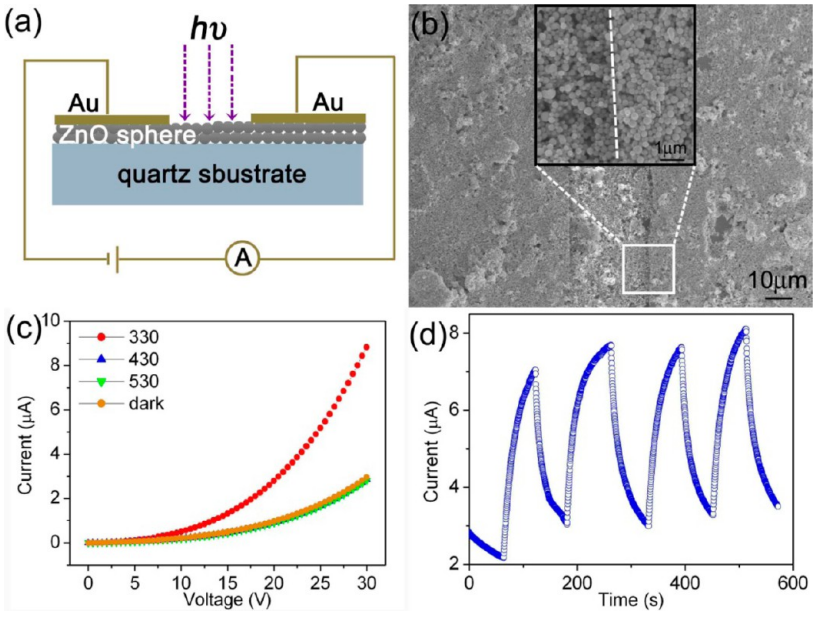

Figure 6. (a) Scheme of the microdevice used for measuring the photocurrent of a film of ZnO spherical particles. (b) Representative SEM image of a ZnO -based photodetector. The inset is a high magnification SEM image of the labelled area. (c) $I-V$ characteristics of ZnO spherical particles illuminated with light of different wavelengths and under dark conditions. (d) On/off switching of a ZnO photodetector under 330 nm illumination measured for the light-on and light-off conditions at a bias of 30.0 V.

shown in Figure 6b. The Au parallel electrodes with a 30 μm gap (visible from the depth difference shown in Figure 6d) were deposited on the spherical particles dispersed on a quartz substrate, and the uncovered ZnO was exposed to the light. The inset of Figure 6b shows the high-magnification SEM image of the boundary (dashed line) between the Au-covered and Au-uncovered parts.

Figure 6c shows the $I-V$ curves of the ZnO spherical particle based photodetector exposed to light with different wavelengths and at darkness. Compared with the dark current, the photocurrent with illumination at 330 nm increases by more than 4 timesand further enhancement can be obtained by applying a high bias voltage. Additionally, the photodetector exhibits wavelength selectivity, since no obvious photocurrent can be observed when choosing longer wavelengths such as 430 nm and 530 nm. The photocurrent response of the ZnO spherical particle photodetector is shown in Figure 6d, which is measured under the period of 330 nm light on and off conditions at a bias voltage of 30.0 V. The present photodetector is stable and reproducible. As we just simply coated the spherical particles on the substrate and did not make further annealing treatment, which might lead to non-close-contact between particles and substrate, slight changes of off-current are observed in Figure 6d.

The photoconduction mechanism includes the generation of free carriers and the electrical transport within spherical particles, through the interface between neighbouring spheres and the metal/ZnO interface. It should be mentioned herein that the photocurrent generated in a film of ZnO single-crystalline spheres is higher than that reported for polycrystalline spheres.[11−13] The reason for this may be, on the one hand, the increased electronic conductivity due to the single crystalline nature of the spheres, which eliminates the barriers for electron transfer within spherical particles. On the other hand, the "clean" surface (without carbon, Figure 2e), favors the electrical transport through the interface between neighbouring spheres.

CONCLUSIONS

In conclusion, the formation and UV photodetection ability of single-crystalline ZnO spherical particles has been demonstrated. Microstructure analysis of the particles before and after laser irradiation reveals a crystal size increase and shape transformation from irregular to spherical. The unique heating mode involved in pulsed laser irradiation allows for maintenance of the spherical shape of the melted particles upon pulsed light absorption. Surface carbon is removed by laser irradiation, and surface adsorption of carbon by resultant spherical particles is reduced due to the smooth surfaces. Time dependent laser irradiation most probably causes fusion of nanoparticles to enable growth up to larger single crystalline spherical particles. High sensitivity of the resultant spherical ZnO particles towards ultraviolet light is achieved. This is considered to originate from, on the one hand, the increased electronic carrier mobility due to the single crystalline nature of the spheres, and on the other hand, the "clean" surface caused by carbon ablation by the pulsed laser. Our study reveals the potential of nanosecond pulsed lasers in generating crystalline spherical particles for optoelectronic applications.

AUTHOR INFORMATION

Corresponding Author

*E-mail: Hongqiang.Wang@mpikg.mpg.de.

Notes

The authors declare no competing financial interest.

ACKNOWLEDGMENTS

This work was partially supported by Grants-in-Aid for Scientific Research (B) (20360340). H.W. acknowledges the support of a research fellowship from the Alexander von Humboldt Foundation. Dr. L. Li is acknowledged for his help with photodetection measurement.

REFERENCES

(1) Lieber, C. M.; Wang, Z. L. Functional Nanowires. *MRS Bull.* **2007**, *32*, 99−108.

(2) Fang, X. S.; Bando, Y.; Shen, G. Z.; Ye, C. H.; Gautam, U. K.; Costa, P. M. F. J.; Zhi, C. Y.; Tang, C. C.; Golberg, D. Ultrafine ZnS Nanobelts as Field Emitters. *Adv. Mater.* **2007**, *19*, 2593−2596.

(3) Peng, L.; Hu, L. F.; Fang, X. S. Low-Dimensional Nanostructure Ultraviolet Photodetectors. *Adv. Mater.* **2013**, *25*, 5321−5328.

(4) Wang, H. Q.; Li, G. H.; Jia, L. C.; Wang, G. Z.; Li, L. General in situ Chemical Etching Synthesis of ZnO Nanotips Array. *Appl. Phys. Lett.* **2008**, *93*, 153110−1-3.

(5) Li, L.; Wu, P. C.; Fang, X. S.; Zhai, T. Y.; Dai, L.; Liao, M. Y.; Koide, Y.; Wang, H. Q.; Bando, Y.; Golberg, D. Single-Crystalline CdS Nanobelts for Excellent Field-Emitters and Ultrahigh Quantum-Efficiency Photodetectors. *Adv. Mater.* **2010**, *22*, 3161−3165.

(6) Li, L.; Lee, P. S.; Yan, C.; Zhai, T. Y.; Fang, X. S.; Liao, M. Y.; Koide, Y.; Bando, Y.; Golberg, D. Ultrahigh-Performance Solar-Blind Photodetectors Based on Individual Single-Crystalline $In_2Ge_2O_7$ Nanobelts. *Adv. Mater.* **2010**, *22*, 5145−5149.

(7) Xia, F.; Mueller, T.; Lin, Y.; Valdes-Garcia, A.; Avouris, P. Ultrafast Graphene Photodetector. *Nat. Nanotechnol.* **2009**, *4*, 839−843.

(8) Taniyasu, Y.; Kasu, M.; Makimoto, T. An Aluminium Nitride Light-Emitting Diode with A Wavelength of 210 Nanometres. *Nature* **2006**, *441*, 325−328.

(9) Fang, X. S.; Bando, Y.; Liao, M.; Zhai, T. Y.; Gautam, U. K.; Li, L.; Koide, Y.; Golberg, D. An Efficient Way to Assemble ZnS Nanobelts as Ultraviolet-Light Sensors with Enhanced Photocurrent and Stability. *Adv. Funct. Mater.* **2010**, *20*, 500−508.

(10) Fang, X. S.; Hu, L. F.; Huo, K. F.; Gao, B.; Zhao, L. J.; Liao, M. Y.; Chu, P. K.; Bando, Y.; Golberg, D. New Ultraviolet Photodetector Based on Individual Nb2O5 Nanobelts. *Adv. Funct. Mater.* **2011**, *21*, 3907−3915.

(11) Wang, X.; Liao, M. Y.; Zhong, Y.; Zheng, J. Y.; Tian, W.; Zhai, T. Y.; Zhi, C. Y.; Ma, Y.; Yao, J. N.; Bando, Y.; Golberg, D. ZnO Hollow Spheres with Double-Yolk Egg Structure for High-Performance Photocatalysts and Photodetectors. *Adv. Mater.* **2012**, *24*, 3421−3425.

(12) Tian, W.; Zhang, C.; Zhai, T. Y.; Li, S. L.; Wang, X.; Liao, M. Y.; Tsukagoshi, K.; Golberg, D.; Bando, Y. Flexible SnO_2 Hollow Nanosphere Film based High-performance Ultraviolet Photodetector. *Chem. Commun.* **2013**, *49*, 3739−3741.

(13) Chen, M.; Hu, L. F.; Xu, J.; Liao, M. Y.; Wu, L. M.; Fang, X. S. ZnO Hollow-Sphere Nanofilm-Based High-Performance and Low-Cost Photodetector. *Small* **2011**, *7*, 2449−2453.

(14) Wang, Y.; Xia, Y. Bottom-Up and Top-Down Approaches to the Synthesis of Monodispersed Spherical Colloids of Low Melting-Point Metals. *Nano Lett.* **2004**, *4*, 2047−2050.

(15) Jeong, U.; Wang, Y.; Ibisate, M.; Xia, Y. Some New Developments in the Synthesis, Functionalization, and Utilization of Monodisperse Colloidal Spheres. *Adv. Funct. Mater.* **2005**, *15*, 1907−1921.

(16) Cobley, M. C.; Rycenga, M.; Zhou, F.; Li, Z. Y.; Xia, Y. N. Controlled Etching as a Route to High Quality Silver Nanospheres for Optical Studies. *J. Phys. Chem. C* **2009**, *113*, 16975−16982.

(17) Lee, Y. J.; Schade, N. B.; Sun, L.; Fan, J. A.; Bae, D. R.; Mariscal, M. M.; Lee, G.; Capasso, F.; Sacanna, S.; Manoharan, V. N.; Yi, G. R.

Ultrasmooth, Highly Spherical Monocrystalline Gold Particles for Precision Plasmonics. *ACS Nano* **2013**, *7*, 11064−11070.
(18) Wang, H. Q.; Pyatenko, A.; Kawaguchi, K.; Li, X.; Swiatkowska-Warkocka, Z.; Koshizaki, N. Selective Pulsed Heating for the Synthesis of Semiconductor and Metal Submicrometer Spheres. *Angew. Chem., Int. Ed.* **2010**, *49*, 6361−6364.
(19) Wang, H. Q.; Miyauchi, M.; Ishikawa, Y.; Pyatenko, A.; Koshizaki, N.; Li, Y.; Li, L.; Li, X.; Bando, Y.; Golberg, D. Single-Crystalline Rutile TiO_2 Hollow Spheres: Room-Temperature Synthesis, Tailored Visible-Light-Extinction, and Effective Scattering Layer for Quantum Dot-Sensitized Solar Cells. *J. Am. Chem. Soc.* **2011**, *113*, 19102−19109.
(20) Wang, H. Q.; Jia, L.; Li, L.; Li, X.; Swiatkowska-Warkocka, Z.; Kawaguchi, K.; Pyatenko, A.; Koshizaki, N. Photomediated Assembly of Single Crystalline Silver Spherical Particles with Enhanced Electrochemical Performance. *J. Mater. Chem. A* **2013**, *1*, 692−698.
(21) Li, X. Y.; Pyatenko, A.; Shimizu, Y.; Wang, H. Q.; Koga, K.; Koshizaki, N. Fabrication of Crystalline Silicon Spheres by Selective Laser Heating in Liquid Medium. *Langmuir* **2011**, *27*, 5076−5080.
(22) Umar, A.; Kim, B. K.; Kim, J. J.; Hahn, Y. B. Optical and Electrical Properties of ZnO Nanowires Grown on Aluminium Foil by Non-Catalytic Thermal Evaporation. *Nanotechnology* **2007**, *18*, 175606−1-7.
(23) Chantarat, N.; Chen, Y. W.; Chen, S. Y.; Lin, C. C. Enhanced UV Photoresponse in Nitrogen Plasma ZnO Nanotubes. *Nanotechnology* **2009**, *20*, 395201−1-5.
(24) Zheng, X. J.; Yang, B.; Jiang, C. B.; Mao, S. X.; Chen, Y. Q.; Yuan, B. Enhancement in Ultraviolet Optoelectronic Performance of Photoconductive Semiconductor Switch Based on ZnO Nanobelts Film. *Appl. Phys. Lett.* **2009**, *95*, 221106−1-3.
(25) Wang, H. Q.; Jia, L. C.; Bogdanoff, P.; Fiechter, S.; Möhwald, H.; Shchukin, D. Size-related Native Defect Engineering in High Intensity Ultrasonication of Nanoparticles for Photoelectrochemical Water Splitting. *Energy Environ. Sci.* **2013**, *6*, 799−804.
(26) Wang, H. Q.; Koshizaki, N.; Li, L.; Jia, L. C.; Kawaguchi, K.; Li, X. Y.; Pyatenko, A.; Swiatkowska-Warkocka, Z.; Bando, Y.; Golberg, D. Size-Tailored ZnO Submicrometer Spheres: Bottom-Up Construction, Size-Related Optical Extinction, and Selective Aniline Trapping. *Adv. Mater.* **2011**, *23*, 1865−1870.
(27) Fujiwara, H.; Niyuki, R.; Ishikawa, Y.; Koshizaki, N.; Tsuji, T.; Sasaki, K. Low-Threshold and Quasi-Single-Mode Random Laser within a Submicrometer-Sized ZnO Spherical Particle Film. *Appl. Phys. Lett.* **2013**, *102*, 061110−1-4.
(28) Ishikawa, Y.; Katou, Y.; Koshizaki, N.; Feng, Q. Raw Particle Aggregation Control for Fabricating Submicrometer-sized Spherical Particles by Pulsed-laser Melting in Liquid. *Chem. Lett.* **2013**, *42*, 530−531.
(29) Pyatenko, A.; Yamaguchi, M.; Suzuki, M. Mechanisms of Size Reduction of Colloidal Silver and Gold Nanoparticles Irradiated by Nd:YAG Laser. *J. Phys. Chem. C* **2009**, *113*, 9078−9085.
(30) Pyatenko, A.; Yamaguchi, M.; Suzuki, M. Synthesis of Spherical Silver Nanoparticles with Controllable Sizes in Aqueous Solutions. *J. Phys. Chem. C* **2007**, *111*, 7910−7917.
(31) Pyatenko, A.; Wang, H.; Koshizaki, N.; Tsuji, T. Mechanism of Pulse Laser Interaction with Colloidal Nanoparticles. *Laser Photonics Rev.* **2013**, *7*, 596−604.
(32) Yoshikawa, H.; Adachi, S. Optical Constants of ZnO. *Jpn. J. Appl. Phys.* **1997**, *36*, 6237−6243.
(33) Wang, H. Q.; Kawaguchi, K.; Pyatenko, A.; Li, X. Y.; Swiatkowska-Warkocka, Z.; Katou, Y.; Koshizaki, N. General Bottom-Up Construction of Spherical Particles by Pulsed Laser Irradiation of Colloidal Nanoparticles: A Case Study on CuO. *Chem.—Eur. J.* **2012**, *18*, 163−169.
(34) Pyatenko, A.; Yamaguchi, M.; Suzuki, M. Laser Photolysis of Silver Colloid Prepared by Citric Acid Reduction Method. *J. Phys. Chem. B* **2005**, *109*, 21608−21611.
(35) McGrath, T. E.; Diebold, G. J.; Bartels, D. M.; Crowell, R. A. Laser-Initiated Chemical Reactions in Carbon Suspensions. *J. Phys. Chem. A* **2002**, *106*, 10072−10078.
(36) Soci, C.; Zhang, A.; Xiang, B.; Dayeh, S. A.; Aplin, D. P. R.; Park, J.; Bao, X. Y.; Lo, Y. H.; Wang, D.; ZnO Nanowire, U. V. Photodetectors with High Internal Gain. *Nano Lett.* **2007**, *7*, 1003−1009.